Theoretical Study of Low-Spin, High-Spin, and Intermediate-Spin States of $[Fe^{III}(pap)_2]^+$ (pap = N-2-pyridylmethylidene-2-hydroxyphenylaminato). Mechanism of Light-Induced Excited Spin State Trapping

Hideo Ando,[†] Yoshihide Nakao,[†] Hirofumi Sato,[†] and Shigeyoshi Sakaki*[,†,‡]

Department of Molecular Engineering, Graduate School of Engineering, Kyoto University, Nishikyo-ku, Kyoto 615-8510, Japan, and Fukui Institute for Fundamental Chemistry, Kyoto University, Nishi-hiraki cho, Takano, Sakyo-ku, Kyoto 606-8301, Japan

Received: February 19, 2007; In Final Form: April 21, 2007

The mechanism of light-induced excited spin state trapping (LIESST) of $[Fe^{III}(pap)_2]^+$ (pap = N-2-pyridylmethylidene-2-hydroxyphenylaminato) was discussed on the basis of potential energy surfaces (PESs) of several important spin states, where the PESs were evaluated with the DFT(B3LYP) method. The PES of the quartet spin state crosses those of the doublet and sextet spin states around its minimum. This means that the spin transition occurs from the quartet spin state to either the doublet spin state or the sextet spin state around the PES minimum of the quartet spin state. The PES minimum of the sextet spin state is slightly less stable than that of the doublet spin state by 0.18 eV (4.2 kcal/mol). This small energy difference is favorable for the LIESST. The doublet-sextet spin crossover point is 0.41 eV (9.6 kcal/mol) above the PES minimum of the sextet spin state. Because of this considerably large activation barrier, the thermal spin transition and the tunneling process do not occur easily. In the doublet spin state, the ligand to ligand charge transfer (LLCT) transition is calculated to be 2.16 eV with the TD-DFT(B3LYP) method, in which the π orbital of the phenoxy moiety and the π^* orbital of the imine moiety in the pap ligand participate. This transition energy is moderately smaller than the visible light of 550 nm used experimentally. In the sextet spin state, the ligand to metal charge transfer (LMCT) transition is calculated to be at 2.36 eV, which is moderately higher than the visible light (550 nm). These results indicate that the irradiation of the visible light induces the LIESST to generate the sextet spin state but the reverse-LIESST is also somewhat induced by the visible light, indicating that the complete spin conversion from the doublet spin state to the sextet one does not occur, as reported experimentally.

Introduction

Spin crossover phenomenon induced by photoirradiation, which is called light-induced excited spin state trapping (LIESST), was first experimentally reported by Gütlich et al. in 1984.[1] Since then, the LIESST has drawn considerable interests because it is expected to be utilized for optical molecular switch.[2−7] However, the transition-metal complexes that exhibit the LIESST have been limited to several iron(II) complexes.[1−5,7−9] To understand well the LIESST and to find a new LIESST compound, we need the detailed knowledge of the mechanism of the LIESST.

In general, it is believed that the LIESST occurs through spin-allowed d−d excitation followed by two steps of intersystem crossing via the intermediate-spin (IS) state.[1c,2−4] For example, the mechanism of the LIESST of iron(II) complex was proposed as follows (Scheme 1).[1c] First, the low-spin (LS) excited state, either $^1T_{1g}$ or $^1T_{2g}$, is generated from the LS ground state, $^1A_{1g}$, by photoirradiation. Then, part of the complexes in the LS excited states decay to the LS ground state through internal conversion, and the remaining part change to the IS states such as $^3T_{1g}$ and $^3T_{2g}$ through intersystem crossing. The excited IS states rapidly decay to the lowest-energy IS state, $^3T_{1g}$, through internal conversion. Finally, this state converts either to the LS ground state, $^1A_{1g}$, or to the lowest-energy high-spin (HS) state, $^5T_{2g}$, through intersystem crossing. Because the intersystem crossing is involved as important process in the LIESST, it was

SCHEME 1: Proposed Mechanism of the LIESST in the d^6 Iron(II) Complex

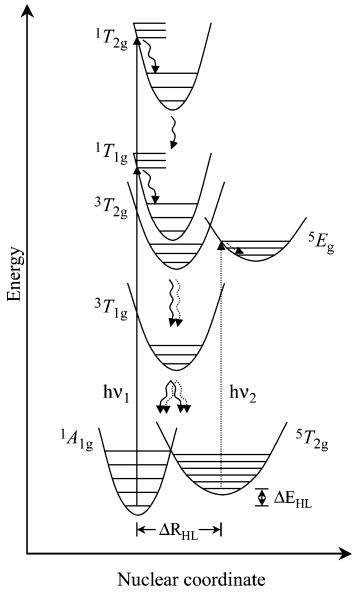

* Corresponding author. E-mail: sakaki@moleng.kyoto-u.ac.jp.
† Graduate School of Engineering.
‡ Fukui Institute for Fundamental Chemistry.

10.1021/jp0714163 CCC: $37.00
Published on Web 06/05/2007

SCHEME 2: Schematic Pictures of PESs of the Low-Spin (LS), High-Spin (HS), and Intermediate-Spin (IS) States

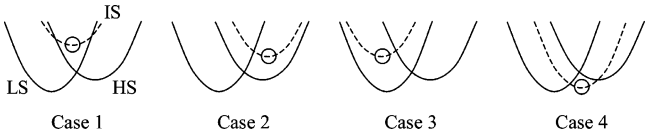

investigated in detail by several groups.[10−13] Also, we must remember that the LIESST does not occur totally if the lowest-energy HS state easily converts to the LS ground state through tunneling process, thermal activation, and/or reverse-LIESST.[4a,6,8,10−13] To suppress the tunneling and thermal processes, the potential wall for spin transition must be sufficiently high and wide. In other words, the geometrical difference between the LS ground state and the lowest-energy HS state, ΔR_{HL}, must be large, and their energy difference, ΔE_{HL}, must be small.[8b,11,13b,d]

Thus, detailed knowledge of the potential energy surfaces (PESs) of the LS, HS, and IS states is indispensable to understand the LIESST mechanism and to synthesize a new LIESST compound. For instance, following issues should be theoretically clarified: what excited state is generated by photoirradiation, whether the excited LS states convert to the IS states, whether the lowest-energy IS state converts to the LS ground state or the lowest-energy HS state, and how much easily (or with difficulty) the thermal spin transition and tunneling process occur between the LS ground state and the lowest-energy HS state.

It had been believed for long that iron(II) complexes exhibit the LIESST because of the large ΔR_{HL} value but iron(III) complexes cannot exhibit it in general because of the small ΔR_{HL} value.[2,6,8b,11,13b,d] Recently, however, Hayami, Sato, and their collaborators reported that an iron(III) complex, $[Fe^{III}(pap)_2]^+$ (pap = N-2-pyridylmethylidene-2-hydroxyphenylaminato) exhibits the LIESST.[6,14] This observation is against the general understanding that the iron(III) complexes are not useful for the LIESST.[2,6] Thus, it is of considerable interest to investigate the reason why this iron(III) complex exhibits the LIESST.

To understand the LIESST, many theoretical works of iron(II) complexes have been carried out,[14−24] and many of them discussed the relative stabilities of the LS ground state and the lowest-energy HS state. However, the PESs of the LS, HS, and IS states have not been evaluated theoretically in spite of their importance to understand the LIESST. In particular, the PES of the lowest-energy IS state is very important. One of key factors is the position of its energy minimum relative to the PESs of the lowest-energy HS state and the LS ground state. For instance, to induce the LIESST, the PES minimum of the lowest-energy IS state should be above the PES of the lowest-energy HS state, as shown in case 1 and case 2 (Scheme 2). If not, as shown in case 3 and case 4, the intersystem crossing from the lowest-energy IS state to the lowest-energy HS state cannot occur.

In this work, we theoretically investigated geometries and electronic structures of $[Fe^{III}(pap)_2]^+$ by the DFT(B3LYP) and TD-DFT(B3LYP) methods. Our purposes here are to evaluate the relative stabilities of the doublet, sextet, and quartet spin states, to present the PESs of these states, and to clarify the LIESST mechanism of this iron(III) complex.

Computational Details

Geometry of $[Fe^{III}(pap)_2]^+$ was optimized by the DFT method in the lowest-energy doublet (LS), sextet (HS), and quartet (IS) spin states, where B3LYP functional[25,26] was used. The excitation energies of $[Fe^{III}(pap)_2]^+$ were evaluated by the TD-DFT-(B3LYP) method.

In geometry optimization, usual LANL2DZ[27] basis set of double-ζ quality was used for Fe, where its core electrons (up to 2p) were replaced with effective core potentials (ECPs). For the other atoms, cc-pVDZ[28] basis sets were employed. This basis set system is named BS-I here. Important geometries were recalculated with better basis sets. For Fe, (5311/5311/311/1)[27,29,30] and (7511/6711/411/1)[29−31] basis sets were used with the ECPs of Hay-Wadt and Christiansen groups, respectively, where these are of double-ζ quality for valence s and p electrons and of triple-ζ quality for valence d electrons. A (311111/22111/411/1)[32] basis set of triple-ζ quality was also used for Fe with the ECPs of Stuttgart group. In all these basis sets, one f-polarization function was added; see Supporting Information Tables S1 for details of these basis sets. For the other atoms, either cc-pVDZ or cc-pVTZ[28] basis sets were employed; combination of these basis sets will be shown in Table 2. Also, B3LYP* functional[33] was used to calculate several important geometries, because this functional well reproduces the energy splitting of various spin states of $Fe(phen)_2(NCS)_2$.[17] In this calculation, the (311111/22111/411/1) basis set with the ECPs of Stuttgart group and the cc-pVTZ basis sets were employed for Fe and the other atoms, respectively. In the calculation of the transition energy with the TD-DFT method, the same basis set was used for Fe and the cc-pVDZ basis sets were employed for the other atoms.[34]

It is not easy to evaluate PESs with appropriate coordinates which satisfactorily cover the LS, IS, and HS states, because very complicated geometry changes occur among these states. Here, we evaluated PESs in an approximate manner using linear internal coordinates,[35] which is similar to linear transit procedure[36] as follows: The set of internal coordinates (α_i^A; $i = 1$ to $3N - 6$, where N is the number of atoms) in one spin state A is varied linearly to the set of internal coordinates (α_i^B) in another spin state B. When the transit takes place in n steps, the internal coordinate at the mth step is determined by adding the difference $\Delta\alpha_i^m \{= m(\alpha_i^B - \alpha_i^A)/n\}$ to α_i^A. This procedure was previously used to evaluate PESs of reactions of transition-metal complexes.[37,38]

Though $[Fe^{III}(pap)_2]ClO_4$ exists in molecular crystal,[6,14] we did not consider the influence of such neighbors as counter anions and the other complexes in the crystal.

All the DFT and TD-DFT calculations were carried out with Gaussian 03 program package[39] and the MRMP2 calculations were performed with GAMESS program package.[40] Molecular orbitals were drawn with MOLEKEL program package.[41]

TABLE 1: Selected Geometrical Parameters (Bond Lengths and Their Changes (Å)) of $[Fe^{III}(pap)_2]^+$ Optimized with the B3LYP/BS-I Method

bonds	doublet	quartet	sextet	ΔR_{HL}
$Fe-O^1$	1.869 (1.882)[a]	1.949	1.921 (1.931)[a]	0.053 (0.049)[a]
$Fe-O^2$	1.869 (1.883)	1.868	1.921 (1.932)	0.053 (0.049)
$Fe-N^1$	1.934 (1.915)	2.084	2.195 (2.136)	0.261 (0.221)
$Fe-N^2$	1.934 (1.911)	1.963	2.195 (2.105)	0.261 (0.194)
$Fe-N^3$	2.019 (1.993)	2.311	2.252 (2.138)	0.233 (0.145)
$Fe-N^4$	2.019 (1.994)	2.049	2.252 (2.202)	0.233 (0.208)

[a] Experimental values.[14c]

Results and Discussion

Geometries of $[Fe^{III}(pap)_2]^+$ in the Doublet, Quartet, and Sextet Spin States. We optimized geometries of $[Fe^{III}(pap)_2]^+$ in the lowest-energy doublet, quartet, and sextet spin states. As

TABLE 2: Relative Energies (eV)[a] of the Doublet, Quartet, and Sextet Spin States at Various Geometries (see Figures 3 and S2)

functional	B3LYP						B3LYP*
basis set	BS-I	BS-II	BS-III	BS-IV	BS-V	BS-VI	BS-VI
Fe	Hay-Wadt (341/311/41)	Hay-Wadt (5311/5311/311/1)	Hay-Wadt (5311/5311/311/1)	Christiansen (7511/6711/411/1)	Stuttgart (311111/22111/411/1)	Stuttgart (311111/22111/411/1)	Stuttgart (311111/22111/411/1)
others	cc-pVDZ	cc-pVDZ	cc-pVTZ	cc-pVDZ	cc-pVDZ	cc-pVTZ	cc-pVTZ
				(A) Geometry of the Doublet Spin State			
doublet	0.00	0.00	0.00	0.00	0.00	0.00	0.00
quartet	1.14	1.09	1.05	1.04	1.02	0.99	1.08
sextet	1.58	1.43	1.34	1.34	1.29	1.23	1.44
				(B) Geometry of the Quartet Spin State			
doublet	0.54	0.56	0.57	0.51	0.51	0.52	0.56
quartet	0.61	0.59	0.57	0.49	0.48	0.48	0.58
sextet	0.73	0.60	0.53	0.46	0.42	0.40	0.62
				(C) Geometry of the Sextet Spin State			
doublet	1.43	1.48	1.52	1.37	1.36	1.41	1.49
quartet	0.88	1.03	1.12	0.93	0.81	0.90	1.12
sextet	0.18	0.10	0.09	−0.06	−0.10	−0.06	0.15

[a] The doublet spin state at the optimized geometry was taken to be standard (energy zero).

SCHEME 3: $[Fe^{III}(pap)_2]^+$

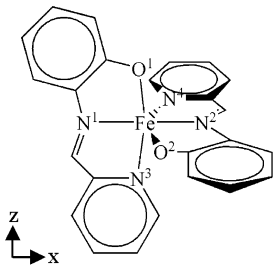

shown in Table 1 (see also Supporting Information Figure S1), the Fe−O and Fe−N distances of the lowest-energy doublet spin state agree well with the experimental values.[14c] It is noted that the Fe−N^3 and Fe−N^4 distances are longer than the Fe−N^1 and Fe−N^2 distances, where the N^1 and N^2 atoms are involved in the imine moiety and the N^3 and N^4 atoms are in the pyridine moiety (see Scheme 3 for N^1, N^2, O^1, etc.). One reason of the longer Fe−N^3 and Fe−N^4 bonds is the strong trans-influence effect of the anionic O atom of the phenoxy moiety.

In this lowest-energy doublet spin state, the d_1 orbital on the O^1−O^2−N^3−N^4 plane is singly occupied (see Figure 1(A) for d_1, d_2, etc.), because the d_1 orbital is destabilized in energy by the antibonding interaction with the doubly occupied p orbitals of the O^1 and O^2 atoms (see Scheme 4); see also Supporting Information Table S2 for the other doublet spin states.

In the quartet spin state, the Fe−O^1 distance becomes longer than that of the doublet spin state, while the Fe−O^2 distance is almost the same. The Fe−N^1 and Fe−N^3 distances are considerably longer and the Fe−N^2 and Fe−N^4 distances are moderately longer than those of the doublet spin state. These changes are interpreted in terms of occupation of d orbitals as follows: In the doublet spin state, two e_g-like d_σ orbitals are unoccupied, one t_{2g}-like d_π orbital is singly occupied, and the other two t_{2g}-like d_π orbitals are doubly occupied, as shown in Figure 1(A). In the quartet spin state, one e_g-like d_σ orbital becomes singly occupied while it is unoccupied in the doublet spin state, and one more t_{2g}-like d_π orbital becomes singly occupied while it is doubly occupied in the doublet spin state, as shown in Figure 1(B). Of the two d_σ orbitals, the d_4 orbital becomes singly occupied and the d_5 orbital is still unoccupied.[42] As a result, the Fe−O^1 and Fe−N^3 distances are considerably longer in the quartet spin state than in the doublet spin state, while the Fe−O^2 and Fe−N^4 distances little change. Though the N^1 lone pair orbital does not form very large antibonding overlap with the d_4 orbital, the Fe−N^1 distance is considerably longer in the quartet spin state than in the doublet spin state. This is interpreted as follows: The O^1 and N^3 atoms moderately move toward $-x$ direction to decrease the antibonding overlap with the d_4 orbital (see Scheme 3 for the coordinates), which induces the Fe−N^1 bond lengthening because the N^1, N^3, and O^1 atoms are in the same pap ligand.

In the sextet spin state, the optimized Fe−O^1 and Fe−O^2 distances agree well with the experimental values,[14c] while the Fe−N^1 and Fe−N^4 distances are moderately longer and the Fe−N^2 and Fe−N^3 distances are considerably longer than the experimental values, as shown in Table 1. Though the considerable discrepancies in the Fe−N^2 and Fe−N^3 distances between the optimized and experimental geometries seem to suggest the geometry optimization is not performed well, our computational results are considered reasonable as follows: Because all the five d orbitals are singly occupied in the sextet spin state, the Fe−N^1 and the Fe−N^3 distances should be the same as the Fe−N^2 and the Fe−N^4 distances, respectively, as shown by the optimized geometry. On the other hand, the Fe−N^3 distance is much different from the Fe−N^4 distance and the Fe−N^1 distance is somewhat different from the Fe−N^2 distance in the experimental geometry. It is likely that these bond distances are considerably influenced by the counteranion and/or the crystal packing.

All the bond distances are longer in the sextet spin state than in the doublet spin state; for instance, the Fe−N^1 and Fe−N^2 distances are 1.934 Å in the doublet spin state but 2.195 Å in the sextet spin state, and the Fe−N^3 and Fe−N^4 distances are 2.019 Å in the doublet spin state but 2.252 Å in the sextet spin state. These geometry differences between the doublet and sextet spin states result from the fact that e_g-like d_4 and d_5 orbitals are unoccupied in the doublet spin state but singly occupied in the sextet spin state. Also, the difference in bond distance between the doublet and sextet spin states, ΔR_{HL}, is similar to the experimental value except for the Fe−N^2 and Fe−N^3 bonds.[43] It is noted that the averaged value of ΔR_{HL}(Fe−N) is not different very much between the optimized value (0.247 Å) and the experimental one (0.192 Å).[14c]

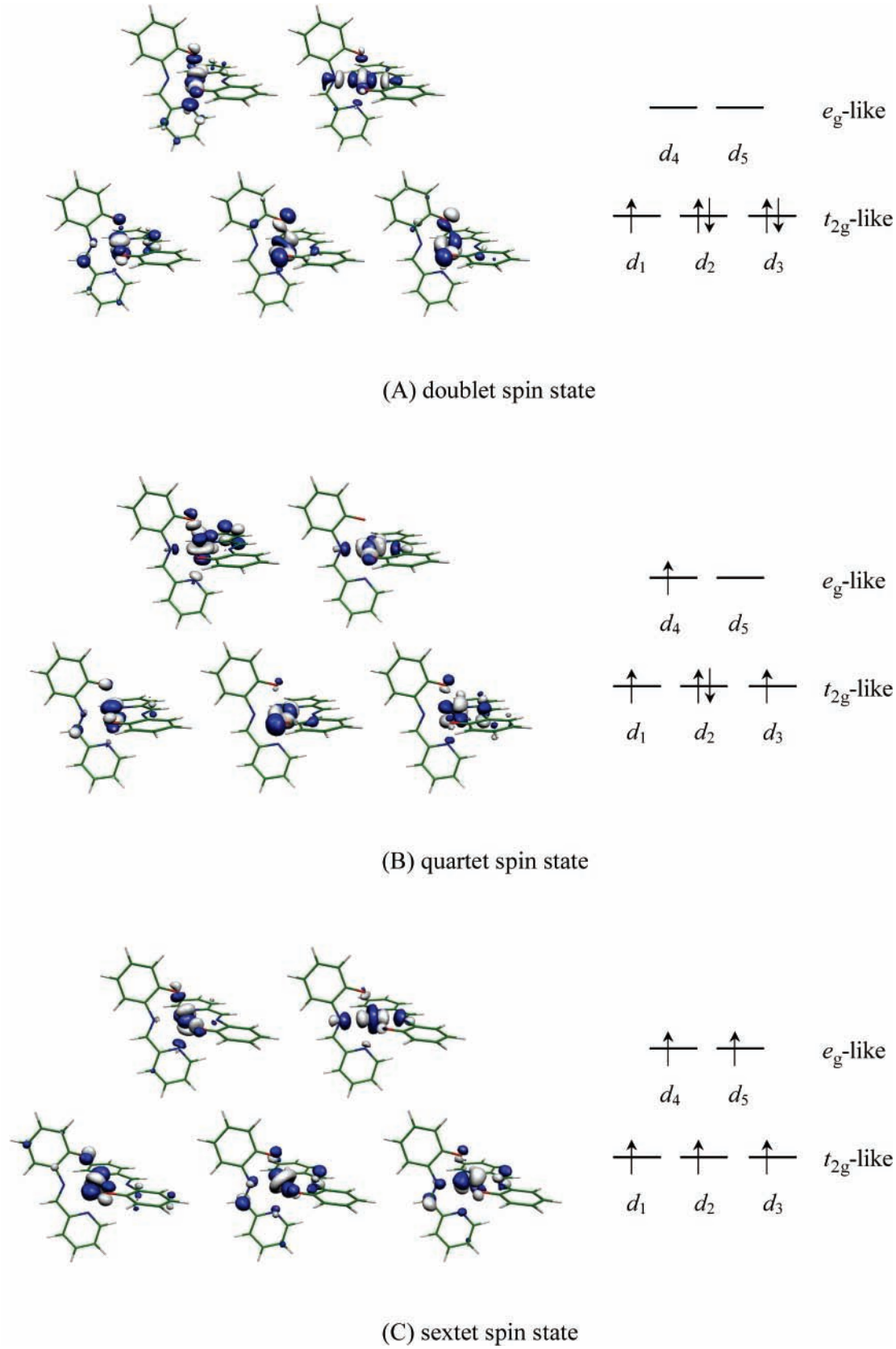

Figure 1. The d orbitals of $[Fe^{III}(pap)_2]^+$. The π and π^* orbital energies of the pap ligand are between the t_{2g}- and the e_g-like orbital energies.

In $[Fe^{II}(pap)_2]$, the similar bond lengthening is induced by spin state change from the singlet spin state to the quintet spin state (see Supporting Information Table S3). The bond lengthening occurs considerably larger in $[Fe^{II}(pap)_2]$ than in $[Fe^{III}(pap)_2]^+$ as expected.[2,6]

In summary, these optimized geometries agree with the experimental ones in most cases, and the geometry changes induced by spin transition are consistent with our expectation. Thus, we will present our discussion based on these optimized geometries.

SCHEME 4

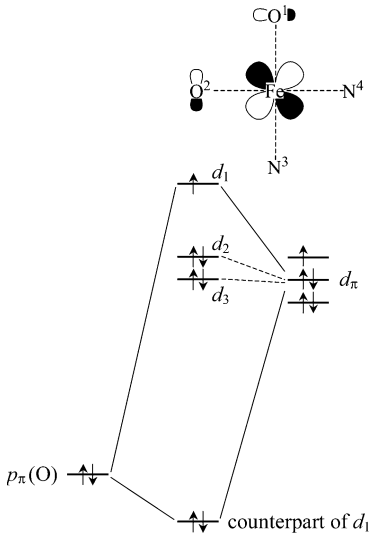

Potential Energy Surfaces along Geometry Changes from the Equilibrium One of the Doublet Spin State to That of the Quartet Spin State. At the equilibrium geometry of the doublet spin state, the quartet and sextet spin states are 1.14 and 1.58 eV above the doublet spin state, respectively (see Table 2). At the equilibrium geometry of the quartet spin state, the energy differences among these three states are very small: It is 0.07 eV between the doublet and quartet spin states and 0.12 eV between the quartet and sextet spin states in the calculation with the BS-I. In the calculation with better basis sets, these three states are in almost the same energy, as shown in Table 2 and Figure 3 (see also Figures S2); for example, the above-mentioned energy differences decrease to 0.02 and 0.04 eV, respectively, where the DFT(B3LYP*)/BS-VI method was used (see Table 2 for BS-VI). It is noted that the B3LYP and the B3LYP* functionals present similar energy differences among these states.

When the geometry changes from the equilibrium one of the doublet spin state to that of the quartet spin state, the doublet spin state becomes higher in energy monotonously, while the quartet and sextet spin states become lower in energy monotonously, as shown in Figure 3. These energy changes are easily interpreted in terms of the orbital energy changes. In the quartet spin state, one e_g-like d_4 orbital is singly occupied but it is unoccupied in the doublet spin state (see Figure 1B). This orbital energy becomes lower through the $Fe-O^1$ and $Fe-N^3$ bond lengthening which is induced by the geometry changes from the doublet spin state to the quartet spin state (see above), because the d_4 orbital forms antibonding overlaps with the O^1 and N^3 lone pair orbitals. As a result, the quartet spin state becomes more stable in energy through these geometry changes. Also, the sextet spin state becomes more stable in energy through these geometry changes because of the same reason.

On the other hand, these geometry changes destabilize the doublet spin state in energy as follows: The $Fe-O^1$ and $Fe-N^3$ bond lengthening decreases the bonding overlap of the e_g-like d_4 orbital with the O^1 and N^3 lone pair orbitals. Because the antibonding d_4 orbital is unoccupied and its bonding counterpart is doubly occupied in the doublet spin state, the decrease in the bonding overlap weakens the $Fe-O^1$ and $Fe-N^3$ bonds, to destabilize the doublet spin state.

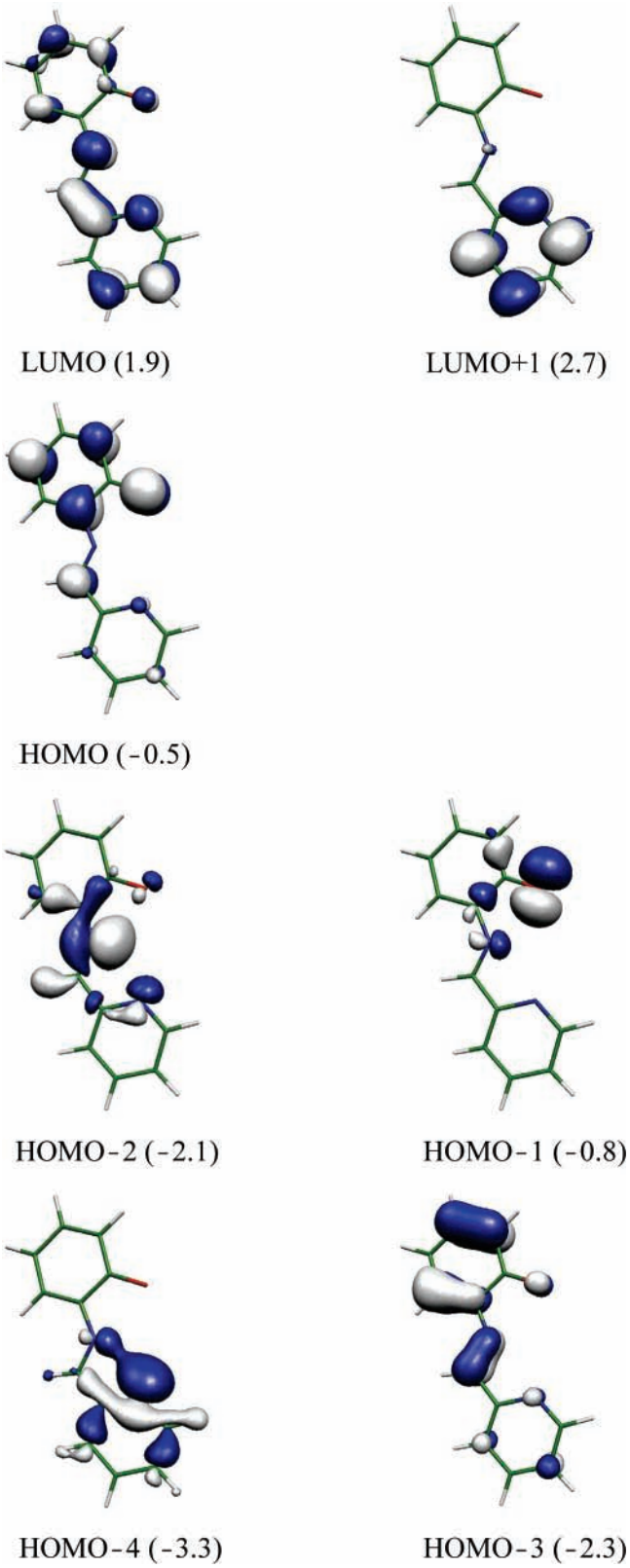

Figure 2. Important molecular orbitals of the pap anion. In parentheses are Kohn−Sham orbital energies (eV).

Potential Energy Surfaces along Geometry Changes from the Equilibrium One of the Quartet Spin State to That of the Sextet Spin State. At the equilibrium geometry of the sextet spin state, the doublet spin state is the least stable in energy and the quartet spin state is the next, as shown in Figure 3 and Table 2. In the calculations with the BS-I, the PES of the sextet spin state crosses those of the doublet and quartet spin states at

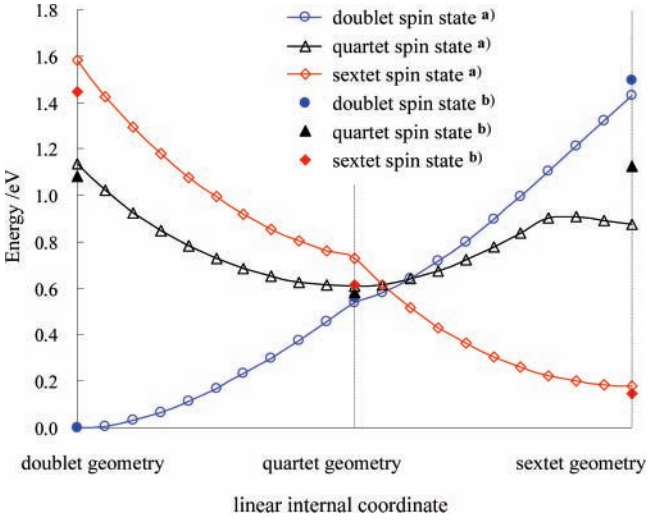

Figure 3. PESs of the doublet, quartet, and sextet spin states of $[Fe^{III}(pap)_2]^+$. (a) The B3LYP/BS−I method. (b) The B3LYP*/BS−VI method. See Table 2 for BS-I, etc.

the geometry that slightly shifts toward the equilibrium one of the sextet spin state from that of the quartet spin state. However, the calculations with better basis sets clearly show that the PESs cross each other around the equilibrium geometry of the quartet spin state (see Figure 3 and Supporting Information Figures S2).

When the geometry changes from the equilibrium one of the quartet spin state to that of the sextet spin state, the sextet spin state becomes more stable in energy, while both of the quartet and doublet spin states become less stable. In these geometry changes, the $Fe-N^1$, $Fe-N^2$, and $Fe-N^4$ distances considerably lengthen and the $Fe-O^2$ distance moderately lengthens, while the $Fe-O^1$ and $Fe-N^3$ distances moderately shorten. The $Fe-O^1$ and $Fe-N^3$ bond shortening raises the e_g-like d_4 orbital energy (see Figure 1(C) for the d_4 orbital), but the $Fe-O^2$ and $Fe-N^4$ bond lengthening lowers the d_4 orbital energy. Thus, the d_4 orbital energy does not change very much. On the other hand, the $Fe-N^1$ and $Fe-N^2$ bond lengthening induces the energy stabilization of the e_g-like d_5 orbital. Because these d_4 and d_5 orbitals are singly occupied, the sextet spin state becomes more stable through these geometry changes. On the other hand, the $Fe-O^2$, $Fe-N^1$, $Fe-N^2$, and $Fe-N^4$ bond lengthening decreases the overlaps of the Fe d orbital with the O^2, N^1, N^2, and N^4 lone pair orbitals, which weakens the $Fe-O^2$, $Fe-N^1$, $Fe-N^2$, and $Fe-N^4$ bonds. As a result, the doublet spin state becomes less stable, because the d_5 orbital is not occupied but its bonding counterpart is doubly occupied in this state. Also, the quartet spin state becomes less stable, because the d_5 orbital is unoccupied in this state like that in the doublet spin state; note that the d_4 orbital is singly occupied in the quartet spin state but its energy level little changes through the geometry changes, as discussed above.

Spin Transition from the Quartet Spin State either to the Sextet Spin State or to the Doublet Spin State. The first step is generation of the doublet excited-state by photoirradiation. Part of the complexes in the doublet excited-state decay to the doublet ground state. The remaining part convert to the quartet spin state through the intersystem crossing. On the PES of the quartet spin state, the geometry changes toward the equilibrium one of the quartet spin state, as shown in Figure 3. The PES of the quartet spin state crosses that of the sextet spin state around the PES minimum of the quartet spin state (see Figure 3). Thus, the intersystem crossing from the quartet spin state to the sextet spin state takes place around the equilibrium geometry of the quartet spin state.

TABLE 3: Excitation Energies (eV) and Oscillator Strengths[a] of $[Fe^{III}(pap)_2]^+$ in the Doublet Spin State

energies (oscillator strengths)	assignments
1.53 (3.0×10^{-4}), 1.57 (0.0×10^{-4})	d−d (d_2, $d_3 \rightarrow d_4$)
1.76 (2.5×10^{-2})	LMCT(Ph [d] $\rightarrow d_1$)
2.16 (2.3×10^{-2}), 2.16 (3.2×10^{-2})[b]	LLCT(Ph) → Im)[c]
2.19 (3.0×10^{-4}), 2.20 (3.0×10^{-4})	d−d (d_2, $d_3 \rightarrow d_5$)[c]
2.48 (6.2×10^{-2}), 2.49 (7.4×10^{-2})	LLCT(Ph → Im)
2.71 (9.6×10^{-3}), 2.73 (1.1×10^{-3})	d−d (d_2, $d_3 \rightarrow d_4$, d_5)
3.25 (2.4×10^{-2}), 3.26 (2.9×10^{-2})	MLCT (d_2, $d_3 \rightarrow$ Im)
3.31 (7.2×10^{-2}), 3.33 (1.1×10^{-1})	LLCT(Ph → Im, Py)
3.35 (7.1×10^{-2}), 3.36 (6.3×10^{-2}), 3.38 (3.9×10^{-2})	MLCT(d_2, $d_3 \rightarrow$ Im)

[a] We omitted here the CT-type transition of which transition dipole is smaller than 0.02. [b] Because two pap ligands separately participate in the LLCT, two transitions are calculated. The transition dipoles are moderately different between them because of the different interaction with the d_π orbital. [c] Visible light used experimentally (about 2.25 eV (550 nm)).[14c,d] [d] Ph, Im, and Py mean phenoxy, imine, and pyridine moieties, respectively.

TABLE 4: Excitation Energies (eV) and Oscillator Strengths[a] of $[Fe^{III}(pap)_2]^+$ in the Sextet Spin State

energies (oscillator strengths)	assignments
1.30 (2.1×10^{-2})	LMCT(Ph → d_3)
2.36 (2.3×10^{-2})	LMCT(Ph → d_1)
2.58 (3.4×10^{-2})	LLCT(Ph → Im)
2.98 (9.5×10^{-2}), 2.98 (9.0×10^{-2})	LMCT(Ph → d_2, d_3)
3.07 (3.7×10^{-2}), 3.10 (2.8×10^{-2})	LMCT(Ph → d_1)
3.47 (2.8×10^{-2}), 3.50 (1.1×10^{-1})	LLCT(Ph → Im, Py)

[a] We omitted here the CT-type transition of which transition dipole is smaller than 0.02.

The PES of the quartet spin state also crosses that of the doublet spin state around the PES minimum of the quartet spin state. This means that the intersystem crossing from the quartet spin state to the doublet spin state takes place around the equilibrium geometry of the quartet spin state, too.

The PES minimum of the sextet spin state is slightly less stable than that of the doublet spin state by 0.18 eV (4.2 kcal/mol). This result satisfies the requirement that ΔE_{HL} should be small for the LIESST. The doublet-sextet spin crossover point is 0.41 eV (9.6 kcal/mol) above the PES minimum of the sextet spin state. This barrier height seems to be enough to suppress the thermal and tunneling spin conversions between the doublet and sextet spin states. It is also noted that these PESs satisfy the condition of case 1, which is necessary for the LIESST (see Scheme 2).

Excitation Energies of the Doublet and Sextet Spin States. It is important to clarify what kind of excitation is induced by photoirradiation. In the doublet spin state, the lowest-energy excitation is $d(t_{2g}) \rightarrow d(e_g)$ transition, of which transition dipole is very small, as expected (see Table 3). The second is the ligand to metal charge transfer (LMCT) transition from the π orbital[44a] of the phenoxy moiety to the Fe center. Though its transition dipole is considerably large, its transition energy is much smaller than the visible light of 550 nm used experimentally.[14c,d] The third is the ligand to ligand charge transfer (LLCT) transition in which one electron excitation occurs from the π orbital[44a] of the phenoxy moiety to the π^* orbital[44b] of the imine moiety in the pap ligand (see Figure 2 for these orbitals). Its transition dipole is considerably large. The second $d(t_{2g}) \rightarrow d(e_g)$ transition is calculated to be at slightly higher energy than the LLCT transition. These two transitions are induced by the visible light of 550 nm. Because of the very small transition dipole of the $d(t_{2g}) \rightarrow d(e_g)$ transition, the LLCT transition mainly participates in the LIESST.

TABLE 5: Excitation Energies (eV) of the Pap[a] Anion Calculated with the TD-DFT and the MRMP2 Methods

	pap		pap with a point charge (+1)		$[Fe^{III}(pap)_2]^+$
assignments	TD-DFT	MRMP2	TD-DFT	MRMP2	TD-DFT
HOMO → LUMO[b]	2.19	1.71	2.25	2.06	2.16, 2.48[c]

[a] The geometry of the pap anion was taken to be the same as that of $[Fe^{III}(pap)_2]^+$ in the doublet spin state. [b] The HOMO mainly consists of the π orbital of the phenoxy moiety. The LUMO mainly consists of the π^* orbital of the imine moiety. [c] See ref 45.

In the sextet spin state, the lowest-energy excitation is the LMCT transition from the π orbital[44a] of the phenoxy moiety to the Fe center, which is calculated to be at 1.30 eV (see Table 4). The second is the LMCT transition from the π orbital[44c] of the phenoxy moiety to the Fe center. This transition is calculated to be at moderately higher energy (2.36 eV) than the visible light (550 nm) used experimentally.

From these results, it is concluded that the visible light of 550 nm induces the LIESST to generate the sextet spin state but it also somewhat induces the reverse-LIESST; in other words, the complete spin transition from the doublet spin state to the sextet one does not occur and the complexes in the doublet spin state remain to some extent, which are consistent with the experimental fact.[14c,d]

Because the LLCT transition plays an important role in the LIESST, we investigated the excitation energy of the pap anion with the TD-DFT and the MRMP2 methods, to check if the TD-DFT method presents reliable results of the photoexcitation energy. The HOMO → LUMO transition of the pap anion corresponds to the first LLCT transition of $[Fe^{III}(pap)_2]^+$.[45] When only the pap anion is calculated, the MRMP2-calcualted transition energy is moderately smaller than the TD-DFT-calculated value, as shown in Table 5. To mimic the positive charge of the Fe(III) center, we investigated the pap anion with one positive charge which was placed at the position of the Fe(III) center of $[Fe^{III}(pap)_2]^+$ in the doublet spin state. The difference in the excitation energy between the TD-DFT and the MRMP2 methods is very small. Also, it is noted that the HOMO → LUMO excitation energy agrees well with the first LLCT excitation energy of $[Fe^{III}(pap)_2]^+$ in the doublet spin state. These results indicate that the TD-DFT method presents reliable excitation energies of $[Fe^{III}(pap)_2]^+$.

Conclusions

Geometry of $[Fe^{III}(pap)_2]^+$ (pap = N-2-pyridylmethylidene-2-hydroxyphenylaminato) was theoretically investigated by the DFT(B3LYP) method in such states as the doublet, quartet, and sextet spin states. All the Fe−O and Fe−N bonds are longer in the sextet spin state than in the doublet spin state. This is because the e_g-like d_4 and d_5 orbitals are unoccupied in the doublet spin state but they are singly occupied in the sextet spin state; remember that the e_g-like d_4 and d_5 orbitals form antibonding overlap with the pap ligand. The ΔR_{HL} values of the iron(III) complex $[Fe(pap)_2]^+$ are smaller than those of the iron(II) complex $[Fe(pap)_2]$, as suggested previously.[2,6]

Potential energy surfaces (PESs) of these spin states were approximately evaluated with the DFT(B3LYP) method, where the geometry changes were estimated by the linear internal coordinate technique. These PESs satisfy case 1 shown in Scheme 2. The PES of the quartet spin state crosses those of the doublet and sextet spin states around its minimum. This means that the quartet spin state converts either to the doublet spin state or to the sextet spin state around the PES minimum of the quartet spin state. The doublet-sextet spin crossover point is calculated to be less stable than the equilibrium geometry of the sextet spin state by 0.41 eV (9.6 kcal/mol). Because of this considerably large barrier height, neither the tunneling process nor the thermal spin conversion occurs easily.

In the doublet spin state, the $d(t_{2g}) \rightarrow d(e_g)$ transition is calculated to be the lowest-energy absorption with the TD-DFT method. The LLCT transition is calculated to be at 2.16 eV as the third absorption, in which one electron transition occurs from the phenoxy moiety to the imine moiety in the pap ligand. The second $d(t_{2g}) \rightarrow d(e_g)$ transition is also calculated to be at 2.19 eV. These two excitations are induced by the irradiation of visible light (550 nm). In the sextet spin state, the LMCT transition is calculated to be at 2.36 eV. This excitation energy is moderately higher than the visible light (550 nm). These results indicate that the irradiation of the visible light (550 nm) induces the LIESST from the doublet spin state to the sextet spin state but the reverse-LIESST is also induced by the visible light, indicating that the complete spin conversion from the doublet spin state to the sextet spin state does not occur and the complexes in the doublet spin state remain to some extent, as experimentally observed.[14c,d] Because of all these factors, the LIESST can be observed in the iron(III) complex, $[Fe(pap)_2]^+$, against the expectation.

Acknowledgment. We acknowledge financial support by Grant-in Aid for Scientific Research on Priority Areas "Molecular Theory" (No.461) and Grant-in Aid for Scientific Research on Basic Area (No.18350005) and on Germination Area (No.17651057) from the Ministry of Education, Science, Culture, and Sports in Japan.

Supporting Information Available: Complete form of ref 39. Scheme of HOMOs of the pap anion in $[Fe^{III}(pap)_2]^+$ (1 page). Table of exponents and coefficients of basis sets (2 page). Table of energies of the doublet spin states (1 page). Table of equilibrium geometry of $[Fe^{II}(pap)_2]$ (1 page). Table of Cartesian coordinates of $[Fe^{III}(pap)_2]^+$ (3 pages). Figure of equilibrium geometries of $[Fe^{III}(pap)_2]^+$ (1 page). PESs of $[Fe^{III}(pap)_2]^+$ calculated with various basis sets (5 pages). This material is available free of charge via the Internet at http://pubs.acs.org.

References and Notes

(1) (a) Decurtins, S.; Gütlich, P.; Köhler, C. P.; Spiering, H.; Hauser, A. *Chem. Phys. Lett.* **1984**, *105*, 1−4. (b) Decurtins, S.; Gütlich, P.; Köhler, C. P.; Spiering, H. *J. Chem. Soc., Chem. Commun.* **1985**, 430−432. (c) Decurtins, S.; Gütlich, P.; Hasselbach, K. M.; Hauser, A.; Spiering, H. *Inorg. Chem.* **1985**, *24*, 2174−2178. (d) Hauser, A.; Gütlich, P.; Spiering, H. *Inorg. Chem.* **1986**, *25*, 4245−4248.

(2) Gütlich, P.; Hauser, A.; Spiering, H. *Angew. Chem., Int. Ed. Engl.* **1994**, *33*, 2024−2054.

(3) Hauser, A.; Jeftić, J.; Romstedt, H.; Hinek, R.; Spiering, H. *Coord. Chem. Rev.* **1999**, *190−192*, 471−491.

(4) (a) Gütlich, P.; Garcia, Y.; Goodwin, H. A. *Chem. Soc. Rev.* **2000**, *29*, 419−427. (b) Gütlich, P.; Garcia, Y.; Woike, T. *Coord. Chem. Rev.* **2001**, *219−221*, 839−879.

(5) In *Molecular Switches*; Feringa, B. L., Ed.; Wiley-VCH: Weinheim, Germany, 2001.

(6) Sato, O. *Acc. Chem. Res.* **2003**, *36*, 692−700.

(7) Bousseksou, A.; Molnár, G.; Matouzenko, G. *Eur. J. Inorg. Chem.* **2004**, *2004*, 4353−4369.

(8) (a) Hauser, A. *Chem. Phys. Lett.* **1986**, *124*, 543−548. (b) Hauser, A. *Chem. Phys. Lett.* **1992**, *192*, 65−70.

(9) Tayagaki, T.; Tanaka, K. *Phys. Rev. Lett.* **2001**, *86*, 2886−2889.

(10) Dose, E. V.; Hoselton, M. A.; Sutin, N.; Tweedle, M. F.; Wilson, L. J. *J. Am. Chem. Soc.* **1978**, *100*, 1141−1147.
(11) Buhks, E.; Navon, G.; Bixon, M.; Jortner, J. *J. Am. Chem. Soc.* **1980**, *102*, 2918−2923.
(12) Xie, C.-L.; Hendrickson, D. N. *J. Am. Chem. Soc.* **1987**, *109*, 6981−6988.
(13) (a) Hauser, A. *J. Chem. Phys.* **1991**, *94*, 2741−2748. (b) Hauser, A.; Vef, A.; Adler, P. *J. Chem. Phys.* **1991**, *95*, 8710−8717. (c) Schenker, S.; Hauser, A. *J. Am. Chem. Soc.* **1994**, *116*, 5497−5498. (d) Schenker, S.; Hauser, A.; Dyson, R. M. *Inorg. Chem.* **1996**, *35*, 4676−4682.
(14) (a) Hayami, S.; Gu, Z.-Z.; Shiro, M.; Einaga, Y.; Fujishima, A.; Sato, O. *J. Am. Chem. Soc.* **2000**, *122*, 7126−7127. (b) Hayami, S.; Sato, O.; Inoue, K.; Einaga, Y.; Maeda, Y. *J. Nucl. Radiochem. Sci.* **2002**, *3*, A1−A9. (c) Juhász, G.; Hayami, S.; Sato, O.; Maeda, Y. *Chem. Phys. Lett.* **2002**, *364*, 164−170. (d) Hayami, S.; Kawahara, T.; Maeda, Y.; Inoue, K.; Sato, O. *J. Radioanal. Nucl. Chem.* **2005**, *266*, 521−525.
(15) Chen, G.; Espinosa-Perez, G.; Zentella-Dehesa, A.; Silaghi-Dumitrescu, I.; Lara-Ochoa, F. *Inorg. Chem.* **2000**, *39*, 3440−3448.
(16) Paulsen, H.; Duelund, L.; Winkler, H.; Toftlund, H.; Trautwein, A. X. *Inorg. Chem.* **2001**, *40*, 2201−2203.
(17) Reiher, M. *Inorg, Chem.* **2002**, *41*, 6928−6935.
(18) Scherlis, D. A.; Estrin, D. A. *Int. J. Quantum Chem.* **2002**, *87*, 158−166.
(19) Kondo, M.; Yoshizawa, K. *Chem. Phys. Lett.* **2003**, *372*, 519−523.
(20) Zhang, Y.; Oldfield, E. *J. Phys. Chem. A* **2003**, *107*, 4147−4150.
(21) Rodriguez, J. H. *J. Chem. Phys.* **2005**, *123*, 094709.
(22) Simaan, A. J.; Boillot, M.-L.; Carrasco, R.; Cano, J.; Girerd, J.-J.; Mattioli, T. A.; Ensling, J.; Spiering, H.; Gütlich, P. *Chem. Eur. J.* **2005**, *11*, 1779−1793.
(23) Daku, L. M. L.; Vargas, A.; Hauser, A.; Fouqueau, A.; Casida, M. E. *ChemPhysChem* **2005**, *6*, 1393−1410.
(24) Brehm, G.; Reiher, M.; Guennic, B. L.; Leibold, M.; Schindler, S.; Heinemann, F. W.; Schneider, S. *J. Raman Spectrosc.* **2006**, *37*, 108−122.
(25) Becke, A. D. *J. Chem. Phys.* **1993**, *98*, 5648−5652.
(26) (a) Lee, C.; Yang, W.; Parr, R. G. *Phys. Rev. B* **1988**, *37*, 785−789. (b) Miehlich, B.; Savin, A.; Stoll, H.; Preuss, H. *Chem. Phys. Lett.* **1989**, *157*, 200−206.
(27) Hay, P. J.; Wadt, W. R. *J. Chem. Phys.* **1985**, *82*, 299−310.
(28) Dunning, T. H., Jr. *J. Chem. Phys.* **1989**, *90*, 1007−1023.
(29) Couty, M.; Hall, M. B. *J. Comput. Chem.* **1996**, *17*, 1359−1370.
(30) One f-polarization function was taken from ref 31.
(31) Hurley, M. M.; Pacios, L. F.; Christiansen, P. A.; Ross, R. B.; Ermler, W. C. *J. Chem. Phys.* **1986**, *84*, 6840−6853.
(32) Dolg, M.; Wedig, U.; Stoll, H.; Preuss, H. *J. Chem. Phys.* **1987**, *86*, 866−872.
(33) Reiher, M.; Salomon, O.; Hess, B. A. *Theor. Chem. Acc.* **2001**, *107*, 48−55.
(34) (a) Because of the large size of $[Fe^{III}(pap)_2]^+$, the cc-pVTZ basis sets could not be used for the ligand atoms in the TD-DFT calculation. We ascertained that the TD-DFT calculation with basis sets of triple-ζ quality presents almost the same results as those of Tables 3 and 4, where the (311111/22111/411/1) basis set with the ECPs of Stuttgart group and Dunning's triple-ζ basis sets[34b] with d-polarization function were used for Fe and the other atoms, respectively; for instance, the first LLCT transition energy of the doublet spin state is 2.14 and 2.15 eV, and the second LMCT transition energy of the sextet spin state is 2.36 eV. (b) Dunning, T. H., Jr. *J. Chem. Phys.* **1971**, *55*, 716−723.
(35) Komornicki, A.; McIver, J. W. *J. Am. Chem. Soc.* **1974**, *96*, 5798−5800.
(36) Salem, L. *Electrons in Chemical Reactions: First Principles*; Wiley: New York, 1982.
(37) (a) Versluis, L.; Ziegler, T.; Baerends, E. J.; Ravenek, W. *J. Am. Chem. Soc.* **1989**, *111*, 2018−2025. (b) Versluis, L.; Ziegler, T. *J. Am. Chem. Soc.* **1990**, *112*, 6763−6768.
(38) The linear transit technique is believed to present upper limit of the energy changes.
(39) Pople, J. A.; et al. *Gaussian 03, Revision C.02*; Gaussian: Inc.: Wallingford, CT, 2004.
(40) Schmidt, M. W.; Baldridge, K. K.; Boatz, J. A.; Elbert, S. T.; Gordon, M. S.; Jensen, J. H.; Koseki, S.; Matsunaga, N.; Nguyen, K. A.; Su, S. J.; Windus, T. L.; Dupuis, M.; Montgomery, J. A. Jr. *J. Comput. Chem.* **1993**, *14*, 1347−1363.
(41) (a) Flükiger, P.; Lüthi, H. P.; Portmann, S.; Weber, J. *MOLEKEL 4.3*; Swiss Center for Scientific Computing: Manno, Switzerland, 2000−2002. (b) Portmann, S.; Lüthi, H. P. MOLEKEL: An Interactive Molecular Graphics Tool. *CHIMIA* **2000**, *54*, 766−770.
(42) When the d_5 orbital is singly occupied instead of the d_4 orbital, the $Fe-O^2$, $Fe-N^1$, $Fe-N^2$, and $Fe-N^4$ distances become longer. We tried to optimize such geometry with the singly occupied d_5 orbital, but the optimized geometry is the same as the present one in which the d_4 orbital is singly occupied. This means that the geometry with the long $Fe-O^2$, $Fe-N^1$, $Fe-N^2$, and $Fe-N^4$ bonds is less stable than that with the long $Fe-O^1$ and $Fe-N^3$ bonds. As a result, the $Fe-O^1$ and $Fe-N^3$ bonds become longer, and the d_4 orbital is singly occupied in the quartet spin state.
(43) It is likely that the $Fe-N^2$ and $Fe-N^3$ distances are influenced by the presence of anion and/or the crystal packing in the sextet spin state, as discussed in the text. Thus, the large discrepancies in $\Delta R_{HL}(Fe-N^2)$ and $\Delta R_{HL}(Fe-N^3)$ between experimental value and computational one do not mean that the geometry optimization is not performed well.
(44) (a) The HOMO of the pap anion is mainly involved. (b) The LUMO of the pap anion is mainly involved. (c) The HOMO-3 of the pap anion is mainly involved.
(45) In $[Fe^{III}(pap)_2]^+$, the HOMO of the pap anion forms in-phase and out-of-phase combinations with the HOMO of the other pap anion (see Supporting Information Scheme S1). $[Fe^{III}(pap)_2]^+$ exhibits the LLCT transitions at 2.16 and 2.48 eV. The out-of-phase combination of HOMOs of the pap anions mainly participates in the former LLCT transition and the in-phase combination mainly participates in the latter one. Because the t_{2g}-like d orbital interacts not with the out-of-phase combination but with the in-phase combination, the former LLCT transition is similar to but the latter one considerably different from the LLCT transition of the pap anion. Here, we compared the former LLCT transition of $[Fe^{III}(pap)_2]^+$ with the LLCT transition of the pap anion.